LA-10604-MS

C.3

Los Alamos National Laboratory is operated by the University of California for the United States Department of Energy under contract W-7405-ENG-36.

Measurement of the High-Energy Leakage Neutron Spectrum from the Little Boy Mockup

Los Alamos
Los Alamos National Laboratory
Los Alamos, New Mexico 87545

LA-10604-MS

UC-46
Issued: November 1985

Measurement of the High-Energy Leakage Neutron Spectrum from the Little Boy Mockup

A. A. Robba

Los Alamos National Laboratory
Los Alamos, New Mexico 87545

CONTENTS

MEASUREMENT OF THE HIGH-ENERGY LEAKAGE NEUTRON SPECTRUM FROM THE LITTLE BOY MOCKUP

A. A. Robba

ABSTRACT

We report measurements of the leakage neutron flux from a mockup of the nuclear device exploded over Hiroshima. Measurements were made at the nose and the waist of the device in the energy range of 1 to 10 MeV using the liquid scintillator NE 213. The technique relies on pulse-shape discrimination to eliminate gamma-ray interactions from the neutron data.

INTRODUCTION

Most of the human exposure data used for setting radiation safety guidelines have been obtained by following the survivors of the nuclear explosions at Hiroshima and Nagasaki. Proper evaluation of these data requires estimates of the radiation exposure received by those survivors. Until now, such estimates were questionable because the device exploded at Hiroshima was never tested and thus no measurements of the leakage neutron flux or neutron spectrum are available. Instead, dose estimates have relied primarily on calculations, which remain unsatisfactory without experimental confirmation. To supply these experimental data, we measured the high-energy leakage neutron spectrum from a mockup[1] of the Little Boy device operating at delayed critical. As can be seen in the photograph of the experimental setup (Fig. 1), measurements were made with the mockup on an outdoor stand to minimize the effect of neutrons returned from the environment.

EXPERIMENT AND METHOD

Neutron flux from the mockup was measured using a 2-in.-diam by 2-in.-high cylindrical NE 213 liquid scintillator detector purchased from Nuclear Enterprises.* The detector was mounted and optically coupled to an RCA-8850 photomultiplier. Because of this detector's sensitivity to gamma rays, we surrounded it with 0.5 in. of lead to reduce the event rate due to gamma-ray interactions in the detector. In addition, we used pulse-shape discrimination (PSD) to identify and later eliminate pulses produced by gamma-ray interactions.

*Nuclear Enterprises. Ltd., Edinburgh, Scotland.

Fig. 1.
The Little Boy mockup on its experimental stand.

It has been shown[2] that in some scintillators that have several scintillating components (for example, the NE 213 scintillator has three scintillating components: 3.16–, 32.3–, and 270–ns), highly ionizing particles deposit a greater fraction of their total light output in the longer lived scintillating components than do less highly ionizing particles. As a result, pulses produced by protons from neutron interactions in the scintillator have more slowly decaying tails than do those produced by electrons from gamma–ray interactions. This difference is commonly used to identify neutron and gamma–ray interactions in scintillators in a variety of ways. Most commonly, the photomultiplier pulse is integrated using a long time constant and then it is double differentiated (delay line and R–C differentiation as well as combinations of both have been used)[3–5] to produce a bipolar pulse in which the zero crossing time is related to the pulse decay time. The time between a constant fraction discriminator trigger and the zero crossing of this pulse is measured to produce a parameter that discriminates between neutron and

gamma–ray interactions. This analog pulse processing is often difficult to adjust and fine tune although good results have been achieved using this technique.

The lack of completely satisfactory, commercially available equipment implementing this technique has led us to use a technique originally suggested by Morris et al.[6] that uses gated charge–integrating analog–to–digital converters (ADCs) to separately integrate the full pulse area and the pulse tail area. Pulses from an RCA–8850 photomultiplier are amplified by a fast photomultiplier amplifier (LeCroy 612AM) so that pulse–shape information is preserved. A constant fraction discriminator then provides the gate for a charge–integrating ADC (LeCroy 2249A). Appropriate cable delays are provided so that the gate and analog pulses arrive at the ADC as shown in Fig. 2. The full pulse area is divided by the pulse tail to produce the parameter used for neutron/gamma–ray discrimination.

To achieve the dynamic range made necessary by the nonlinear light output of NE 213 (light output ~ $E^{3/2}$), the photomultiplier signal is split and data corresponding to three different amplifier gains are acquired simultaneously. Two ADC channels separately integrate the full pulse and the pulse tail for each amplifier gain. A block diagram of the data acquisition electronics appears in Fig. 3. Both the live timer and the gate generator are inhibited during the processing of an earlier gate. Two–parameter data (pulse area and PSD parameter) are acquired by a LeCroy 3500 running a LeCroy 3500–25 fast crate controller to perform CAMAC operations and to do the processing required to obtain the discrimination parameter. Data are stored as a two–parameter histogram: full pulse area (1024 channels) versus gamma–ray discrimination parameter (32 channels).

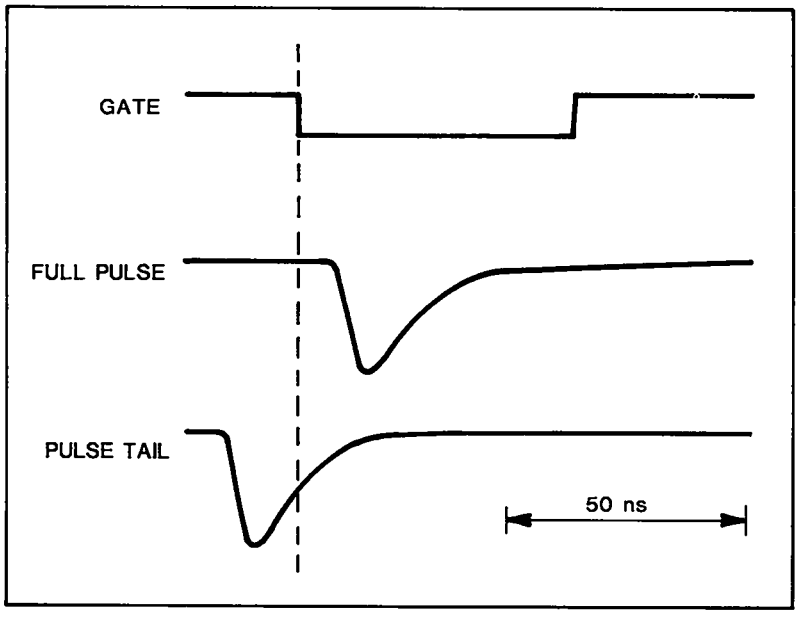

Fig. 2.
Timing of the gate and linear pulses at the ADC.

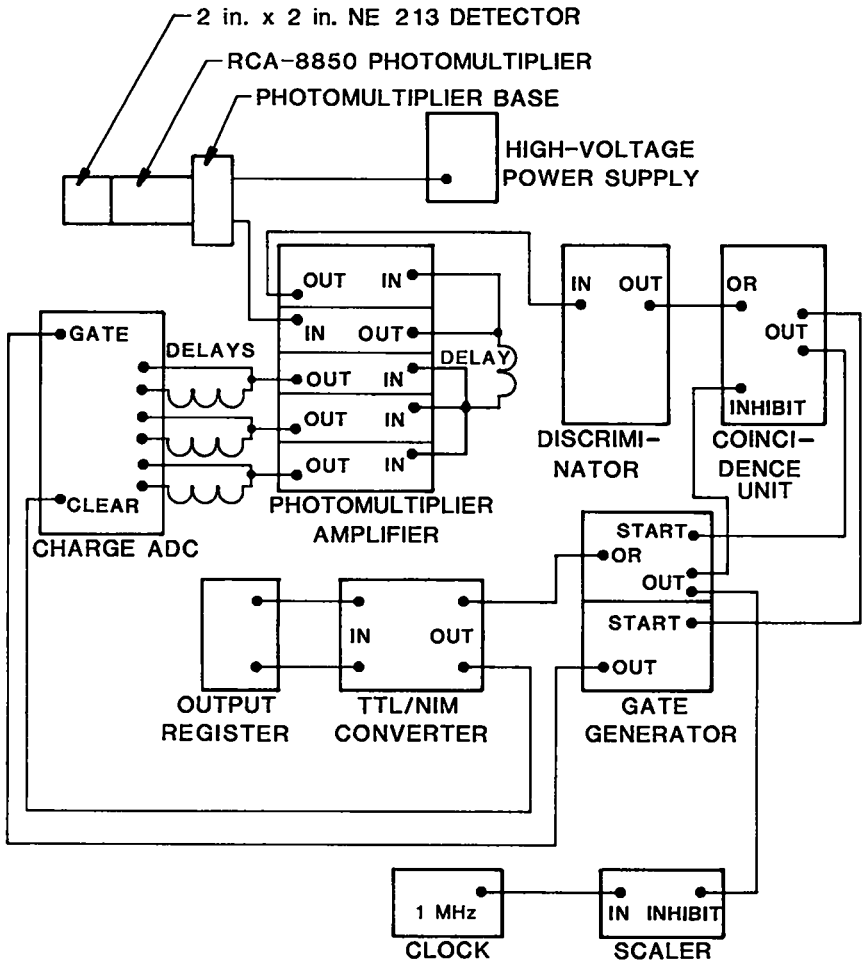

Fig. 3.
Data acquisition electronics.

DATA ANALYSIS

Neutron/gamma-ray separation is accomplished during data analysis. In the dimension of the PSD parameter, the data show two peaks corresponding to neutron and gamma-ray interactions in the scintillator. For each pulse-height channel these peaks are fitted, using the simplex method,[7] by the sum of two Gaussian curves. The parameters of the gamma-ray peak are then used to subtract gamma-ray contamination from the neutron data if there is significant overlap of the two peaks. These peaks are less well separated at low pulse heights and thus this correction for gamma-ray contamination becomes more important there.

The neutron pulse-height data are converted to neutron spectral information using the response functions measured by Verbinski et al.[8]

System gain is calibrated using the half-height point on the upper shoulder of the pulse-height distribution produced by the 1.275-MeV gamma-ray from ^{22}Na. This point on the ^{22}Na spectrum corresponds to 1/1.13 light units.[9] Calibration data in the neighborhood of the 1.275-MeV peak and the half height are each fitted with quadratic curves, which are then used to determine the height of the peak and the location of the half height.

Using this calibration, the measured pulse-height spectra are binned into the same light unit bins as were used by Verbinski in reporting the NE 213 detector's response functions. The neutron spectrum is then obtained by solving the Fredholm integral equation of the first kind, which describes the detector response to an incident neutron flux.

$$D(\xi) = \int_{E_o}^{\infty} dE\ R(E,\xi)\ \phi(E) \quad , \tag{1}$$

where ξ is the pulse height observed from interactions in the detector in light units, E is the incident neutron energy in MeV, $D(\xi)$ is the number of counts observed in the detector as a function of pulse height, $\phi(E)$ is the incident neutron flux on the detector as a function of neutron energy, and $R(E,\xi)$ is the detector response function--the number of counts in $d\xi$ about ξ observed in the detector due to an incident neutron in dE about E.

In practice, D is measured for only a finite number of discrete intervals or ranges of the variable ξ.

$$D_i = \int_{\xi_i}^{\xi_{i+1}} d\xi\ D(\xi) \qquad \text{and} \tag{2}$$

$$D_i = \int_{E_o}^{\infty} dE\ R_i(E)\ \phi(E) \quad , \tag{3}$$

where

$$R_i(E) = \int_{\xi_i}^{\xi_{i+1}} d\xi\ R(\xi,E) \quad . \tag{4}$$

To obtain a set of linear equations that can be solved from the neutron flux, the integration over E is also expressed as a quadrature.

$$D_i = \sum_{j=1}^{J} R_{ij}\phi_j + \varepsilon_i, \text{ for } 1 \le i \le I \quad , \tag{5}$$

or in vector notation,

$$\vec{D} = \vec{R}\vec{\phi} + \vec{\varepsilon} \quad .$$

The matrix R now also contains the quadrature coefficients for the points E_1, E_2, ..., E_j and ξ_1, ..., ε_i represents errors from all sources including that introduced by the quadrature. In this work we have used the following simplest quadrature

$$\int_{E_o}^{\infty} dE\, R_i(E)\, \phi(E) = \sum_{j=1}^{J} R_i(E_j)\, \phi(E_j)\, \Delta E_j = \sum_{j=1}^{J} R_{ij}\, \phi_j \quad , \tag{6}$$

although the formalism applies to any quadrature method.

Equation 5 is overspecified because I, the number of points in which the pulse-height data are available, is larger than J, the number of points at which the neutron flux is obtained. Thus, it seems reasonable to seek a solution by the least squares technique in which we minimize the quantity

$$\chi^2 = \sum_{i=1}^{I} \left(\frac{\varepsilon_i}{\sigma_i} \right)^2 \quad , \tag{7}$$

where σ_i is the estimated error in the measurement D_i. However, it can be shown[10,11] that straightforward solution of this minimization problem is unstable for small errors. This is due to unbounded extraneous solutions that can be introduced into the result by small errors (for example, by roundoff or truncation) and can swamp the desired solution. We have used the "least structure" technique[12,13] to control oscillations while solving for ϕ in Eq. 5. The least structure technique finds the "smoothest" solution consistent with the measured data. It does this by minimizing the square of the numerical approximation for the second derivative of the solution subject to the constraint that $\chi^2 = I$. We introduce the Lagrange multiplier, λ, and minimize the quantity

$$[F(\vec{\phi}) + \lambda^{-1} \chi^2] \quad , \tag{8}$$

where

$$F(\vec{\phi}) = \frac{1}{(\Delta E)^2} \sum_{j=2}^{J-1} \left(\phi_{j+1} - 2\phi_j + \phi_{j-1} \right)^2$$

is a numerical approximation for the second derivative of the solution for the case of equal energy intervals. A similar expression can be derived for the situation of unequal intervals. Setting

$$\frac{\partial}{\partial \phi_k} \; F(\vec{\theta}) + \lambda^{-1} \chi^2 = 0 \quad ,$$

we then obtain

$$\lambda \, \phi_{k+2} - 4\phi_{k+1} + 6\phi_k - 4\phi_{k-1} + \phi_{k-2} + \sum_{i=1}^{I} R_{ik} \, \frac{\epsilon_i}{\sigma_i^2} \quad .$$

By defining the matrices

$$\vec{G} = \begin{bmatrix} 1 & -2 & 1 & & & & & \\ -2 & 5 & -4 & 1 & & & & \\ 1 & -4 & 6 & -4 & 1 & & & \\ & \ddots & \ddots & \ddots & \ddots & \ddots & & \\ & & \ddots & \ddots & \ddots & \ddots & \ddots & \\ & & & \ddots & \ddots & \ddots & \ddots & \ddots \\ & & & & 1 & -4 & 6 & -4 & 1 \\ & & & & & 1 & -4 & 5 & -2 \\ & & & & & & 1 & -2 & 1 \end{bmatrix}$$

and

$$\vec{W} = \begin{bmatrix} \sigma_1^{-2} & & & & & \\ & \sigma_2^{-2} & & & & \\ & & \ddots & & & \\ & & & \sigma_i^{-2} & & \\ & & & & \ddots & \\ & & & & & \sigma_I^{-2} \end{bmatrix}$$

we can then write

$$(\lambda \vec{G} + \vec{R} \cdot \vec{W} \vec{R}) \vec{\phi} = \vec{R} \cdot \vec{W} \vec{D}$$

and the solution is obtained from

$$\vec{\phi} = (\lambda\vec{G} + \vec{R}'\vec{W}\vec{R})^{-1}\ \vec{R}'\vec{W}\vec{D} \quad .$$

LITTLE BOY LEAKAGE SPECTRA

The results from two measurements made at the waist and nose of the Little Boy mockup appear in Figs. 4 and 5. These results are presented without compensation for the effect of the lead used to reduce the gamma-ray event rate in the detector. Both measurements were made with the leakage flux incident on the curved surface of the cylindrical detector reproducing the geometry used by Verbinski in measuring the detector response functions. The distance from the center of the Little Boy core to the centerline of the detector was 2 m for both measurements. For the waist measurement, the detector was at the height of the core center whereas for the nose measurement it was centered on the axis of the mockup, directly above it.

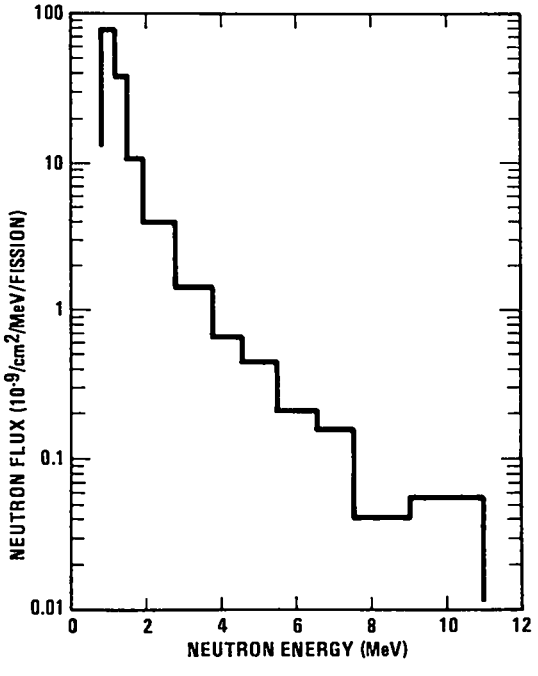

Fig. 4.
Waist measurement of the neutron flux at 2 m from the core center.

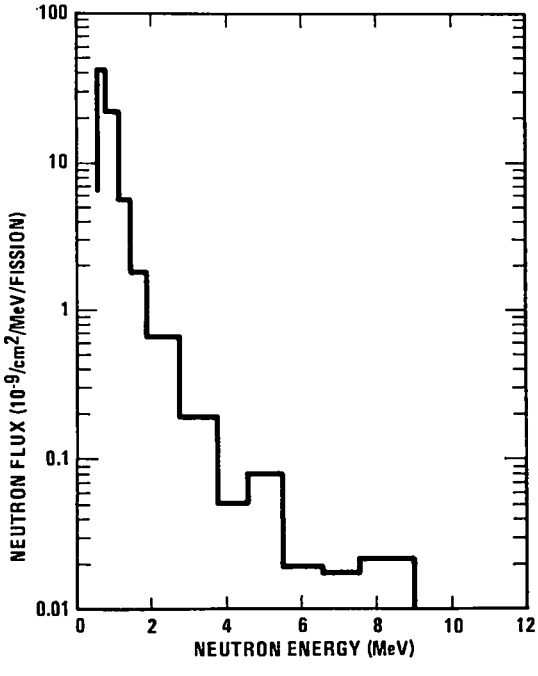

Fig. 5.
Nose measurement of the neutron flux at 2 m from the core center.

The measured neutron flux was normalized to the number of fissions occurring in the mockup using a BF_3 ionization chamber calibrated by Hansen and Forehand.* Foils of ^{235}U (0.001 in. thick) were irradiated in the mockup, after which the fission product, ^{99}Mo, was chemically separated and then counted in a 4π flow counter. Corrections for the flux shape in the mockup were made with the aid of S_n discrete ordinate neutron transport calculations.

Since the measurements reported here were made, data acquisition system improvements have reduced the total processing time per event to approximately 100 μs. With this increased speed, we expect to no longer require the lead gamma-ray shield and to be able to rely on pulse-shape discrimination alone to eliminate gamma-ray events from the data.

These measured spectra provide the best available estimates for the Hiroshima neutron source spectra. Comparisons to a variety of calculations and earlier spectral estimates are now possible. Based on these comparisons, more reliable neutron exposure guidelines should result.

---

*G. E. Hansen and H. M. Forehand, private communication.

REFERENCES

1. R. E. Malenfant, "Little Boy Replication: Justification and Construction," Proceedings of the 17th Midyear Topical Meeting of the Health Physics Society, 1984, Pasco, Washington.

2. F. T. Kuchnir and F. J. Lynch, "Time Dependence of Scintillations and the Effect on Pulse-Shape Discrimination," IEEE Trans. Nucl. Sci. NS-15 (3) (1968).

3. T. K. Alexander and F. S. Goulding, "An Amplitude-Insensitive System that Distinguishes Pulses of Different Shapes," Nucl. Instrum. & Methods 13, 244 (1961).

4. L. Varga, "Pulse Shape Discrimination," Nucl. Instrum. & Methods 14, 24 (1961).

5. M. L. Roush, M. A. Wilson, and W. F. Hornyak, "Pulse Shape Discrimination" Nucl. Instrum. & Methods 31, 112 (1964).

6. C. L. Morris, J. E. Bolger, G. W. Hoffman, C. L. Moore, L. E. Smith, and H. A. Thiessen, "A Ditigal Technique for Neutron-Gamma Pulse Shape Discrimination," Nucl. Instrum. & Methods 137, 397 (1976).

7. J. A. Nelder and R. Mead, "A Simplex Method for Function Minimization," Comput. J. 7, 308 (1965).

8. V. V. Verbinski, W. R. Burrus, T. A. Love, W. Zobel, N. W. Hill, and R. Textor, "Calibration of an Organic Scintillator for Neutron Spectrometry," Nucl. Instrum. & Methods 65, 8 (1968).

9. W. R. Burrus and V. V. Verbinski, Fast Neutron Spectroscopy with Thick Organic Scintillators, "Nucl. Instrum. & Methods 67, 181 (1969).

10. D. L. Philips, "A Technique for the Numerical Solution of Certain Integral Equations of the First Kind," J. Assoc. Comput. Mach. 9, 84 (1962).

11. S. Twomey, "On the Numerical Solution of Fredholm Integral Equations of the First Kind by the Inversion of the Linear System Produced by Quadrature," J. Assoc. Comput. Mach. 10, 97 (1963).

12. B. C. Cook, "Least Structure Solution of Photonuclear Yield Functions," Nucl. Instrum. & Methods 24, 256 (1963).

13. A. A. Robba and L. R. Veeser, "A Least Structure Unfolding Code," Los Alamos Scientific Laboratory report LA-5088 (November 1972).

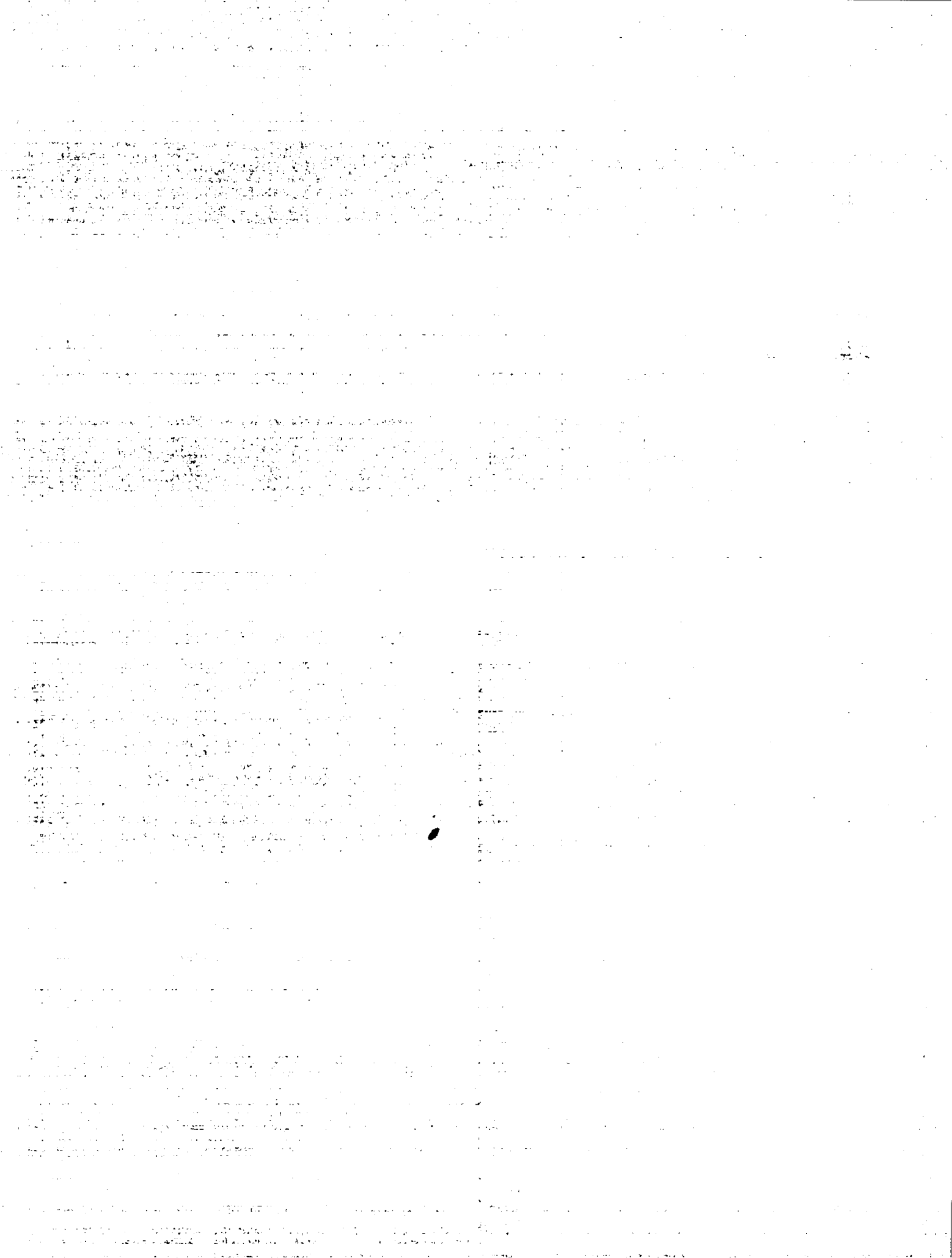

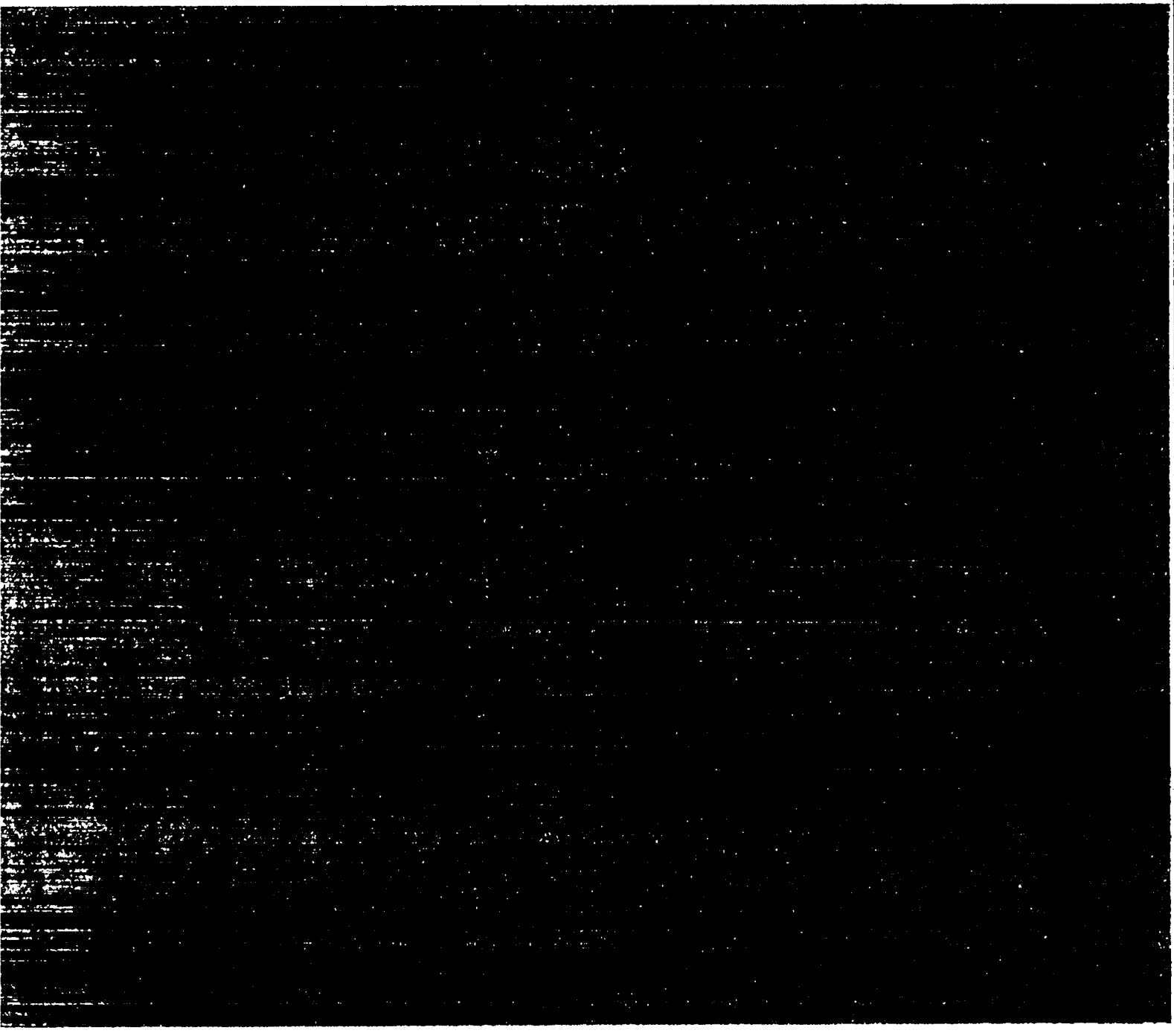

Los Alamos